Production Engineering (2023) 17:613–624
https://doi.org/10.1007/s11740-022-01158-3

PRODUCTION PROCESS

A contribution to the dynamics of the tapping process: analytically estimated and measured instantaneous eigenfrequencies of the tapping tool

Tuğrul Öztürk[1] · Matthias Weigold[1]

Received: 5 June 2022 / Accepted: 1 September 2022 / Published online: 8 September 2022

Abstract
In this contribution an analytical approach for estimating the tapping tool's instantaneous eigenfrequencies of flexural modes is derived. A sensor-integrated tap holder with a close-to-tool vibration sensor attached on the tapping tool is introduced and verified by means of frequency response analysis. The close-to-tool vibration data measured during thread cutting experiments is analyzed in time and frequency domain. The instantaneous eigenfrequencies observed in the spectrogram of the power spectral density are compared with the analytical estimation results. It could be shown that considering for the analytical estimation approach the tapping tool-workpiece contact as clamped boundary condition shows close accordance to the experimental data.

Keywords Tapping · Thread cutting · Tool vibrations · Sensor-integrated tap holder

1 Introduction

The tapping process is still common and widely used for the manufacturing of internal threads as in the aerospace industry for hole threading in jet aero-engine turbine components [1, 2]. Since the tapping process is usually carried out within the last stages of the value chain, the occurrence of uncertainties such as axis offset, tool run-out, synchronization errors or tool breakage can lead to high rework costs or in the worst case even to reject parts [3]. Further, any non-compliance with required thread quality due to progressed tool wear, especially in the aerospace industry where quality standards are crucial, can lead to scrap parts and thus to high economic losses [2]. The contribution is originated from the Collaborative Research Center 805 "Control of Uncertainties in Load Carrying Systems in Mechanical Engineering". The control of uncertainty was investigated within the stages of system design, production, and usage phase within the product life cycle [4]. Focusing on production phase, for detecting uncertainties during the tapping process as a fundamental step of control, a sensor-integrated tap holder was developed allowing the measurement of close-to-tool vibrations [3]. However, detecting uncertainties during the tapping process by means of tool vibrations from a mechanical view forces the comprehension of the dynamic behavior of the cutting tool. As stated in [5] there are few preliminary works about the dynamic analysis of the tapping process, therefore the present contribution intends to reducing this scientific gap. Regarding this, the instantaneous eigenfrequencies of the tapping tool during thread cutting experiments are introduced, which were observed in the time-frequency domain analysis of the close-to-tool vibration data. The results of an analytical approach estimating the instantaneous eigenfrequencies of the tapping tool are compared with experimental data. The present contribution is structured as follows. In Sect. 2 we will state preliminary contributions related to the analysis of the tapping process dynamics as well as vibration-sensor-integrated tool holders available for industrial applications. The analytical approach for estimating the instantaneous eigenfrequencies of the tapping tool's flexural modes is derived in Sect. 3. The introduction of the sensor-integrated tap holder for measuring the close-to-tool vibrations is dedicated to Sect. 4. In Sect. 5

✉ Tuğrul Öztürk
t.oeztuerk@ptw.tu-darmstadt.de

Matthias Weigold
m.weigold@ptw.tu-darmstadt.de

[1] Institute of Production Management, Technology and Machine Tools, Technical University Darmstadt, Otto-Berndt-Straße 2, Darmstadt 69469, Germany

we will first describe the experimental setup following by a comparison and discussion of experimental and analytical results. The contribution ends with conclusions and gives the outlook.

2 State of the art

In this section we will first show preliminary investigations on the dynamics of the tapping process. Further, existing vibration-sensor integrated tool holders for industrial applications are introduced to emphasise the necessity of the developed sensory tap holder presented in this contribution.

Due to the complexity of the tapping process, preliminary contributions about the tapping dynamics are limited. However, Ma et al. [5] made a first attempt to describe the stability of the tapping process using frequency domain methods. First, a dynamic model of the tapping process based on the uncut chip thickness and considering lateral and torsional/axial vibrations was developed. The workpiece-tool contact in radial and rotational direction was modelled by means of spring-damper elements. Based on this dynamic tapping model, a chatter stability prediction model was derived, whereby necessary frequency response functions (FRF) were gained by impact testing of the free tool tip. The chatter stability model was verified by rigid tapping experiments. Further, it could be shown that torsional/axial chatter is the dominant unstable factor in the tapping process.Matsuda et al. [6] have developed a sensor-integrated tool holder system for monitoring rotational vibrations in tapping and end mill process. The vibrations are measured by four accelerometers wich are integrated in the tool holder and circularly arranged at 90° to each other. The vibration signals are acquired and transmitted by on-board electronics such as A/D converter, microcontroller and transmitter. Rotational stick–slip motions could be monitored by the sensor-integrated tool holder during thread cutting experiments on difficult-to-cut materials as Inconel 718. Further, imminent breakage of the tapping tool could be detected by monitoring the vibration signals.

The application of MEMS acceleromers in sensor-integrated tool holders for monitoring edge chipping and edge breakage in milling process is shown in in [7, 8]. Moehring et al. [9] have developed a sensor-integrated milling cutter for predictive process control, whereby a MEMS accelerometer was integrated inside the tool shaft close to the cutting insert. A sensor-integrated floating tap holder for uncertainty detection based on a close-to-tool vibration and an axial length compensation sensor was developed in [3]. Several uncertainty types such as synchronisation error, axis offset, faulty core hole diameter and tap tool breakage could be detected by feature extraction methods in time and frequency domain. Regarding tool breakage, a recent systematic review on tool breakage monitoring techniques in machining operations emphasises that research for tapping process is limited compared to other machining operations such as milling and turning [10].

A sensory tool holder for industrial applications, which measures process vibrations, is the *iTendo*^{2} system manufactured by the company *Schunk*. The *iTendo*^{2} is equipped with one accelerometer, which is integrated in the center axis of the tool holder, thus allowing high speed spindle operations [11].

The sensor-integrated tap holder presented in this contribution is based on a preliminary work shown in [3]. Additionally, the close-to-tool vibration sensor is attached on the tapping tool allowing the measurement of the tool vibrations directly. This is one of the key differences to the state of the art, since the vibration measuring tool holders in the context of research and industry stated here are equipped with accelerometers which are integrated within the tool holder body.

3 Analytical approach for eigenfrequencies estimation of the tapping tool

Before introducing the analytical approach, a few characteristics of the tapping process are stated to emphasise the challenging complexity of the dynamic analysis. The tapping process for manufacturing of internal threads is by nature a complicated machining process [12]. Firstly, the geometry of the tapping tool is more complex compared to tools of other machining operations such as milling or reaming. Multiple cutting edges of the tapping tool are in mechanical contact with the workpiece, whereby the number of cutting edges in contact is depending on the temporal cutting depth. The chip removal for creating the helical groove of the screw thread is carried out by the first cutting edges denoted as the chamfer. The remaining cutting edges are guiding the tapping tool, thus serving as a support [13], shown in Fig. 1. An additional and crucial condition for the tapping process is the synchronisation of the machine tool spindle speed and the feed rate, since the occurrence of synchronisation error can lead to high axial compression or tension forces leading to high amounts of tool wear or even tool breakage [1].

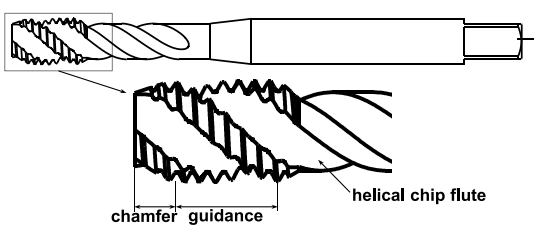

Fig. 1 Segmentation of the tapping tool cutting edges into the chamfer and guidance part

In general, the dynamic behaviour of the cutting tool during machining is characterised not only by the tool dynamics itself, but also by the other components such as the tool holder, the motor spindle and the corresponding interfaces and supports [14]. For the sake of comprehension, Fig. 2 intends to clarify this circumstance by considering the interfaces and supports only and neglecting damping characteristics. First, the dynamics of the motor spindle can be modelled by considering the radial and axial stiffness of the motor spindle bearings $k_{sb,r}$ and $k_{sb,a}$. Further, the tool holder is connected to the motor spindle via the hollow shank taper (HSK) interface represented by the radial and axial stiffness $k_{HSK,r}$ and $k_{HSK,a}$. For manufacturing internal threads with tapping tools, minimal length compensation (MLC) tool holders are usually used, which provide a limited degree of freedom of the tapping tool in longitudinal axis by a linear guided compensating piston [3].

However, according to Fig. 2 the compensating piston is guided in x-axis direction by means of a ball bearing interface which is considered by the radial stiffness $k_{g,r}$. The limited degree of freedom in x-axis direction is mainly determined by cylindrical spring elements made of elastomeric material represented by k_p, which may cause significant nonlinearity in the dynamic characterisation due to viscoelastic material behaviour [15]. Next, the tapping tool is connected to the compensating piston of the MLC tool holder by a collet chuck interface represented by $k_{tc,r}$ and $k_{tc,a}$. The mechanical contact between the tapping tool and the workpiece can be considered by radial and axial spring stiffness as shown in the contribution [5]. It should be clear now, that the dynamic behaviour of the cutting tool is influenced by other components such as tool holder and motor spindle due to interface or bearing stiffness properties.

Since this contribution intends the introduction of an analytical approach for estimating the tapping tool's flexural eigenfrequencies only, the system boundary shown in Fig. 2 comprises the workpiece, the tapping tool and the collet chuck interface, which is assumed as infinitely rigid.

To estimate the tapping tool eigenfrequencies of the flexural modes, the tool geometry is simplified by considering it as a beam system. Hence, the beam system is segmented into three beam parts with constant diameter, due to variable cross section $A(x)$ and second moment of area $I(x)$ along the longitudinal axis of the beam as shown in Fig. 3. The flexural deflection of a beam along the longitudinal axis x at the time t in y-axis direction can be described by a scalar function $w(x, t)$. By neglecting external loads, rotary-inertia and assuming an infinite shear rigidity, the equation of motion for the *Euler-Bernoulli*-beam is governed by considering the equilibrium of forces by means of a differential beam element [16] as follows:

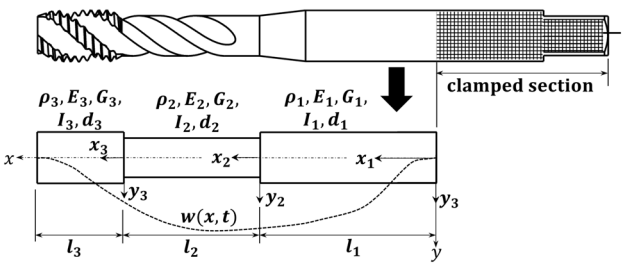

Fig. 3 Simplification of the tapping tool in means of a segmented beam system

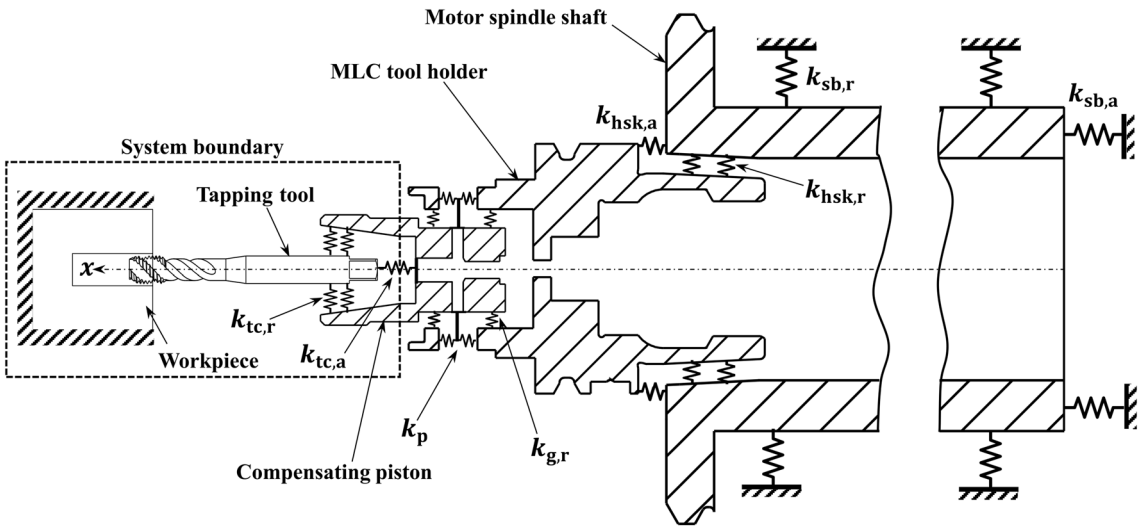

Fig. 2 Modeling approach for the dynamic behavior of the tapping process

$$EI\frac{\partial^4 w(x,t)}{\partial x^4} + \rho A\frac{\partial^2 w(x,t)}{\partial t^2} = 0$$

Since the beam system is segmented into three parts, considering the local coordinate systems $\{x,y\}_i$ yields three homogenous hyperbolic partial differential equations (PDE) which are coupled by means of continuity conditions.

$$E_i I_i \frac{\partial^4 w_i(x_i,t)}{\partial x_i^4} + \rho_i A_i \frac{\partial^2 w_i(x_i,t)}{\partial t^2} = 0 \tag{1}$$

The PDEs (1) are solved by the *Fourier* method (separation of the variables), thus assuming the solution as:

$$w_i(x_i,t) = X_i(x_i)T(t) = X_i(x_i)e^{\mathrm{i}\omega t}\ \forall i \in [1,2,3]$$

whereby for all beam segments a complex exponential basis function $e^{\mathrm{i}\omega t}$ with common ω is considered for the time function $T(t)$. Utilizing the *Fourier* method and considering only the spatial function $X_i(x_i)$ by factoring out the exponential basis function reduces the PDEs (1) into a set of ordinary differential equations (ODEs) of fourth order

$$X_i^{(4)}(x_i) - \beta_i^4 X_i(x_i) = 0 \tag{2}$$

with $\beta_i^4 := \frac{\rho_i A_i}{E_i I_i}\omega^2$ and the n-th spatial derivative $(\cdot)^{(n)} := \frac{\mathrm{d}^{(n)}(\cdot)}{\mathrm{d}x_i^{(n)}}$.

The general solution of the ODEs (2) is given by

$$X_i(x_i) = C_{i1}\sin(\beta_i x_i) + C_{i2}\cos(\beta_i x_i) + C_{i3}\sinh(\beta_i x_i) + C_{i4}\cosh(\beta_i x_i)$$

whereby the constants C_{ij} are determined by boundary and continuity conditions [16].

For the sake of simplicity, a function $t_{i,j}(\beta_i x)$ is introduced:

$$t_{i,j}(\beta_i x) := \begin{cases} \sin(\beta_i x) & \text{if } j = 1 \\ \cos(\beta_i x) & \text{if } j = 2 \\ \sinh(\beta_i x) & \text{if } j = 3 \\ \cosh(\beta_i x) & \text{if } j = 4 \end{cases}$$

Considering $t_{i,j}(\beta_i x)$, the general solution can be expressed as

$$X_i^{(n)}(x_i) = \sum_{j=1}^{N=4} C_{ij} t_{i,j}^{(n)}(\beta_i x_i)\ \forall i \in [1,2,3]$$

Applying the boundary and continuity conditions, the equation system can be derived. Starting from the collet chuck interface, which is assumed as infinitely rigid ($k_{\mathrm{tc,r}} \to \infty$) yields two Eqs. (3).

$$\begin{aligned} X_1^{(0)}(0) &= 0 \\ X_1^{(1)}(0) &= 0 \end{aligned} \tag{3}$$

Further, stress concentrations at the stepped junctions of the beam system are neglected to ensure the continuity of deflection $X_i^{(0)}(x_i)$, slope $X_i^{(1)}(x_i)$, bending moment $E_i I_i X_i^{(2)}(x_i)$ and shear force $E_i I_i X_i^{(3)}(x_i)$ [17, 18]. Therefore, the continuity conditions deliver for $n = 0, 1$ and $k = 1, 2$ the Eq. (4).

$$\begin{aligned} X_k^{(n)}(l_k) - X_{k+1}^{(n)}(0) &= 0 \\ E_k I_k X_k^{(n+2)}(l_k) - E_{k+1} I_{k+1} X_{k+1}^{(n+2)}(0) &= 0 \end{aligned} \tag{4}$$

The tapping tool-workpiece contact is considered in this contribution as clamped (**C**) and simply supported (**S-S**) boundary condition for comparison purposes. This yields to Eqs. (5) and (6).

(C):

$$\begin{aligned} X_3^{(0)}(l_3) &= 0 \\ X_3^{(1)}(l_3) &= 0 \end{aligned} \tag{5}$$

(S-S):

$$\begin{aligned} X_3^{(0)}(l_3) &= 0 \\ X_3^{(2)}(l_3) &= 0 \end{aligned} \tag{6}$$

Rewriting the equation sets (3), (4) and (5) for **(C)** or (3), (4) and (6) for **(S-S)** boundary condition as $\boldsymbol{A}\mathbf{c} = \vec{0}$, where **A** is the coefficient matrix and **c** the column vector of the constants C_{ij}, non-trivial solutions can be found when the determinant of the coefficient matrix is vanishing, thus $\det(\mathbf{A}) = 0$. The coefficient matrix **A** considering **(C)** boundary condition is listed in appendix A.

Resubstituting $\beta_i^4 = \frac{\rho_i A_i}{E_i I_i}\omega^2$ for $i = 1, 2, 3$ in the coefficient matrix **A** yields the so-called frequency equation $F(\omega)$, since any $\omega > 0$ satisfying $F(\omega) = 0$ are the eigenfrequencies of the beam system's flexural modes [19], respectively the tapping tool:

$$F(\omega) = \det(\boldsymbol{A}(\omega)) = 0$$

However, the frequency equation $F(\omega)$ of the beam system does not consider the time-variable length of the tapping tool, which is introduced by means of Fig. 4. Since the cutting depth in machining operations is usually designated with z-coordinate, the longitudinal axis of the coordinate system is changed in Fig. 4b–d, which should not lead to confusion in the following. In Fig. 4b, when the tapping tool is not in contact with the workpiece, the tool can be considered as a cantilever beam. When the tapping process begins, the number of cutting and guiding edges establish a contact with the workpiece with increasing contact length,

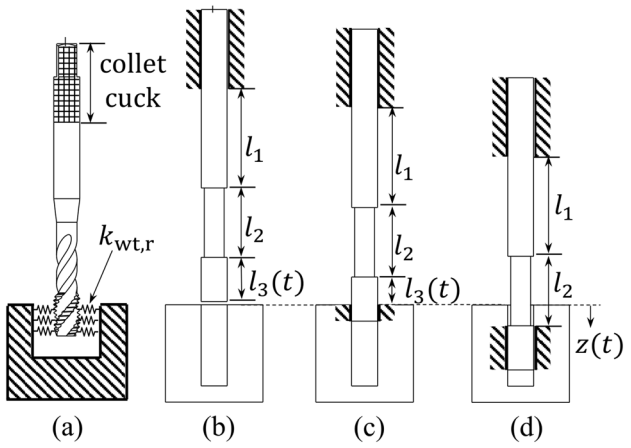

Fig. 4 **a** Workpiece-Tool contact considering radial stiffness only, **b–d** Temporal length of the tapping tool considering clamped boundary condition for workpiece-tool contact

thus yielding a time-variable length of the third beam segment $l_3 = l_3(t)$ illustrated in Fig. 4c. Since the diameter of the second beam segment (chip flute part) is smaller than the thread diameter, the minimum beam system length is reached, when all cutting and guiding edges are in contact with the workpiece expressed by $l_3(t = t^*) = 0$ and shown in Fig. 4d.

The temporal length of the third beam segment $l_3(t)$ is mainly determined by the temporal cutting depth $z = z(t)$. To consider the configurations in Figure 4b-d, the temporal length function $l_3(t)$ is introduced, with $l_{3,0} := l_3(t = 0)$:

$$l_3(t) := \begin{cases} l_{3,0} & \mathrm{z(t)} \leq 0 \\ l_{3,0} - z(t) & 0 < \mathrm{z(t)} \leq l_{3,0} \\ 0 & \mathrm{z(t)} > l_{3,0} \end{cases}$$

Since the beam segment lengths l_1, l_2 and $l_3(t)$ are used within the boundary and continuity conditions, the temporal length function $l_3(t)$ does not violate the application of the Fourier method. Therefore the frequency equation $F\left(\omega, l_3(t)\right)$ considering the temporal length of the tapping tool can be obtained:

$$F\left(\omega, l_3(t)\right) = \det\left(\boldsymbol{A}\left(\omega, l_3(t)\right)\right) = 0$$

The numeric computing environment *MATLAB* was utilized to gain numerical results. The eigenfrequencies of the tapping tool were determined by using the *fzero-function*. The numerical results are based on a high-speed steel blind-hole tapping tool of size M8 from the manufacturer *GARANT*, which is also used for the tapping experiments introduced in Sect. 5. The simplified geometry and material properties of the tapping tool are listed in Table 1. To ensure a consistent temporal length function as in thread cutting

Table 1 Geometry quantities and material properties of beam system, whereby $l_3(t = 0) := l_{3,0} = 13.60\,\mathrm{mm}$

Beam Segment	Young's modulus E_i/GPa	Mass density $\rho_i / \frac{\mathrm{kg}}{\mathrm{m}^3}$	Circular Diameter d_i/mm	Length l_i/mm
1	233	7600	7.94	15.74
2	233	7600	6.10	28.66
3	233	7600	8.00	13.60

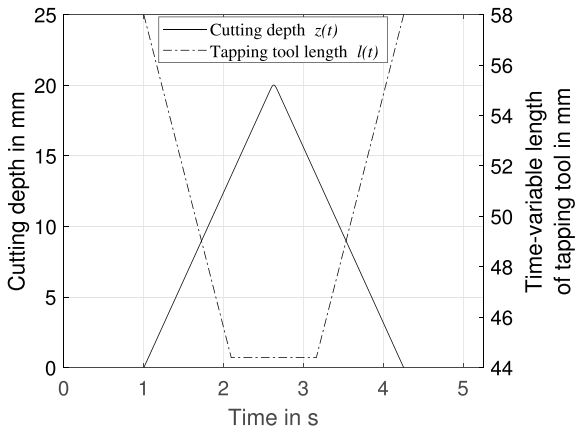

Fig. 5 Temporal cutting depth and tapping tool length

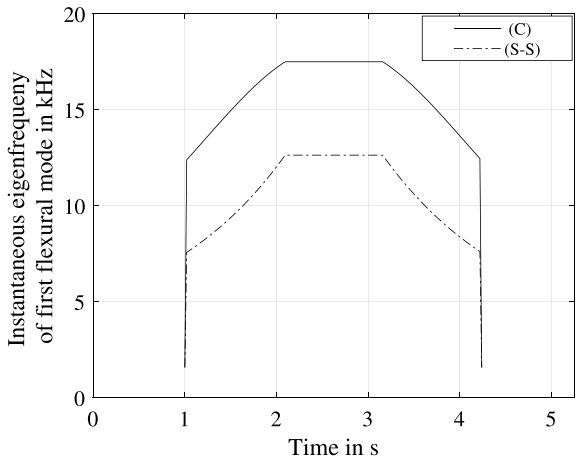

Fig. 6 Instantaneous eigenfrequency of the tapping tools fundamental flexural mode

experiments, the z-position $z(t)$ of the tool center point was obtained from extracted machine internal data. As in the experimental results, the tool center point position is limited to $z_{\max} = 20\,\mathrm{mm}$.

Figure 5 shows the temporal cutting depth $z(t)$ as well as the tapping tool length $l(t) = l_1 + l_2 + l_3(t)$. The instantaneous eigenfrequency of the tapping tool's fundamental flexural mode considering the tool-workpiece contact shown

in Fig. 4a as clamped (**C**) and simply supported (**S-S**) boundary condition is shown in Fig. 6. When the tool-workpiece contact is not established, the tapping tool behaves as a cantilever beam yielding an eigenfrequency of 1.5 kHz. As the tapping process begins, and tool-workpiece contact is established, the eigenfrequency increases to 7, 5 kHz for the **S-S** and 12.3 kHz for **C** boundary condition. With increasing temporal cutting depth $z(t)$, the eigenfrequency is increasing until the plateau is reached, which indicates the entire immersion of the cutting and guiding edges of the tapping tool into the workpiece. The maximum eigenfrequeny is in this state 12.6 kHz for the **S-S** and 17.5 kHz for the **C** boundary condition. One can observe clearly the different slope and curve characteristics of both boundary condition types within the stage of increasing eigenfrequency.

4 Sensor-integrated tapping holder for measuring close-to-tool vibrations

In this section, a brief introduction of the sensor-integrated tap holder is given, which is a further development of the first prototype in a preliminary contribution [3] with regard to downsizing. Further, the working principle and the verification of the close-to-tool vibration sensor is introduced in detail.

As shown in Fig. 7, the sensor-integrated tap holder comprises: (1) tapping tool, (2) close-to-tool vibration sensor, (3) carrier for the telemetry unit with integrated batteries for power supply, (4) a minimal length compensation (MLC) tap holder of type *Softsynchro3* manufactured by the company *Emuge-Franken*, (5) telemetry unit.

For signal processing and data acquisition (DAQ) of the close-to-tool vibration sensor data a telemetry unit was developed. According to the analyticaly estimated eigenfrequencies of the tapping tool in Sect. 3, a multichannel high-speed analog digital converter (ADC) for structural vibration analysis purposes is chosen, providing a high resolution of 24-Bit and a sample rate of 51.2 kHz. The signal processing stage comprises a level adjustment to the ADC and an active low-pass filter of first order to prevent aliasing errors. For simultaneous data acquisition and storing tasks, a 32-bit dual core embedded system based on Xtensa LX6 processors is used, which supports the real-time capable operating system *FreeRTOS*. The integrated WiFi interface within the embedded system enables the remote control of the sensor-integrated tap holder. To prevent any data losses during high speed data acquisition, the bit stream of the ADC is stored on a high speed capable SDCard (SDC) integrated in the telemetry unit. The stored bit stream for data analysis is accessible via download functionality using WiFi.

Figure 8 shows schematically the hardware structure of the telemetry unit considering only one accelerometer of the close-to-tool vibration sensor (CTTVS).

To measure the close-to-tool vibrations, MEMS accelerometers with analog output signal from the semiconductor company *Analog Devices* are used, which provide a linear frequency response function within a wide bandwidth up to 20 kHz, a sensitivity of $20\frac{\text{mV}}{\text{g}}$ and a measuring range of ± 100 g. The structure of the CTTVS is shown in Fig. 9. Since the chosen MEMS accelerometers provide an uniaxial measurement only, two accelerometers (c) were used and arranged perpendicular within the rotational x-y-plane allowing the measurement of the radial accelerations in x- and y-axis direction. Further, the MEMS accelerometers with nearby decoupling capacitors are soldered on a printed circuit board (b) which is bonded via the bottom side to the housing (d) using adhesives. The CTTVS is attached to the tapping tool by a screw connection via a threaded sleeve (a) which is bonded to the tapping tool using adhesives. This type of connection was intentionally chosen to allow a non-destructive application of the CTTVS in case of a tapping tool breakage. It should be mentioned, that the CTTVS is not supported by the tapping tool holder to prevent any stiffening effects.

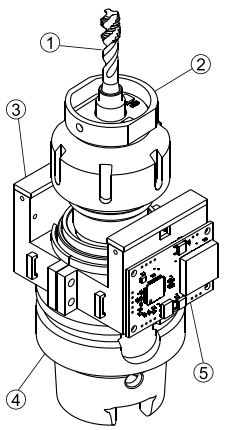

Fig. 7 Sensor-integrated tap holder: (1) tapping tool, (2) CTTVS, (3) telemetry unit carrier with batteries, (5) telemetry unit and (4) MLC

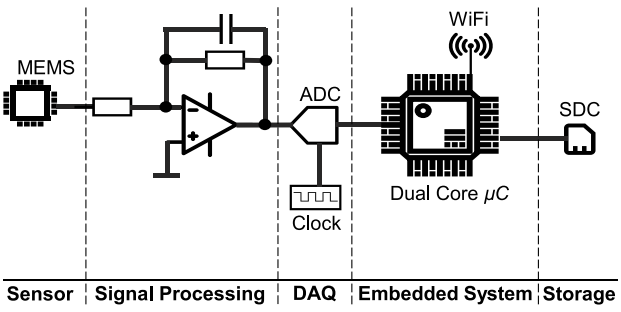

Fig. 8 Schematically structure of the telemetry unit

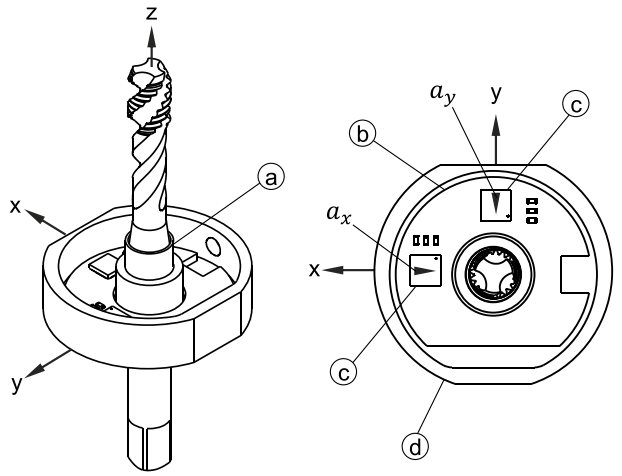

Fig. 9 Structure of the CTTVS: **a** threaded sleeve, **b** printed circuit board, **c** MEMS accelerometers with measuring directions a_x and a_Y as well as **d** sensor housing

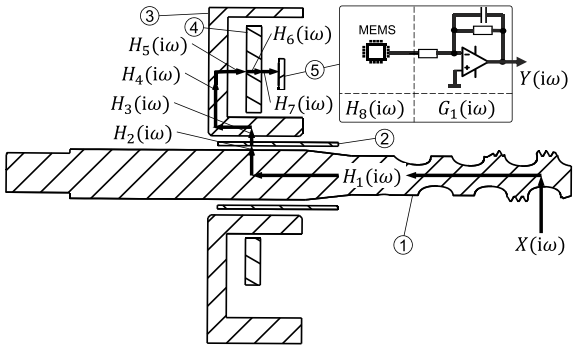

Fig. 10 Propagation of induced tool vibrations to the CTTVS

To provide this condition, the CTTVS is positioned along the z-axis direction in such a way, that even using the entire clamping shank of the tapping tool for the tool holders collect chuck interface, there is a gap between the CTTVS and the tool holder.

The mechanical vibrations which are induced in the tapping tool can be considered as a result of the cutting forces during the chip removal of the chamfer section as well as the frictional forces by the guiding section of the tapping tool, Fig. 1. Therefore the cutting and guiding section of the tapping tool can be considered as the excitation position. Hence, the propagation of the induced vibrations from the excitation position to the MEMS accelerometers (response positions) can be described by means of cascaded (series) transfer functions as shown in Fig. 10 considering one MEMS accelerometer only. The description of the transfer functions are listed in Table 2. Finally, the close-to-tool vibrations $Y(i\omega)$ measured by the MEMS accelerometer which are induced due to the excitation $X(i\omega)$ can be expressed by

$$Y(i\omega) = G_1(i\omega)\left(\prod_{k=1}^{8} H_k(i\omega)\right)X(i\omega)$$

To verify the function of the CTTVS, a free-free experimental frequency response analysis of the sensor-integrated tapping holder including the CTTVS and a reference piezoelectric accelerometer for comparison purposes is used. The top view of the experiment setup is shown in Fig. 11. The sensor-integrated tap holder (9) and the electrodynamic shaker (1) for excitation is supported by elastic ropes to provide free-free boundary conditions. To investigate the influence of the cascaded transfer functions $H_k(i\omega)$ considered for the CTTVS (8), in particular those of the adhesive connections, the frequency response functions (FRF) were obtained by considering two different spatial configurations of the reference accelerometer: (6) Reference accelerometer mounted on the housing of the CTTVS, (5) Reference accelerometer mounted on the tapping tool close to the CTTVS. The electrodynamic shaker is connected via a shaker-stinger (2) and a piezoelectric force transducer (3) to the tapping tool (7) using a customised adapter (4). The adapter contains an internal thread with the same size of the tapping tool, which allows a screwed connection between adapter and tapping tool. To prevent any relative displacement, the adapter is tightened to the tapping tool via a grub screw. This

Table 2 Description of the transfer functions used in Fig. 10

Transfer Function	Description
$H_1(i\omega)$	Tapping tool (1)
$H_2(i\omega)$	Adhesive connection between tapping tool (1) and threaded sleeve (2)
$H_3(i\omega)$	Screw connection between threaded sleeve (2) and sensor housing (3)
$H_4(i\omega)$	Sensor housing (3)
$H_5(i\omega)$	Adhesive connection between sensor housing (3) and printed circuit board (4)
$H_6(i\omega)$	Printed circuit board (4)
$H_7(i\omega)$	Soldered connection between printed circuit (4) board and MEMS accelerometer (5)
$H_8(i\omega)$	MEMS accelerometer (5)
$G_1(i\omega)$	Signal processing stage of the MEMS accelerometer analog output signal

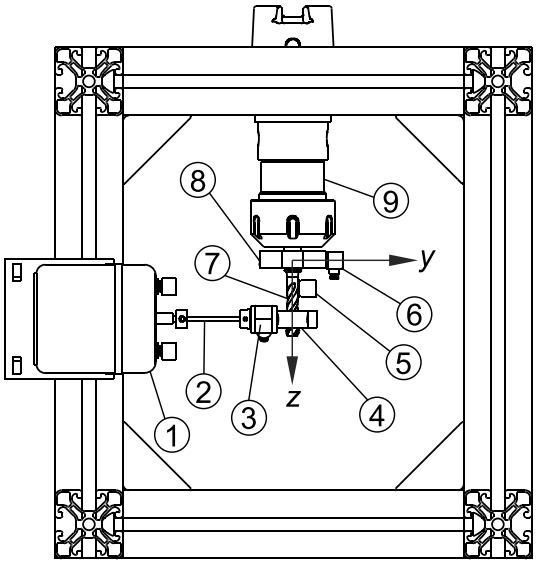

Fig. 11 Test rig for frequency response analysis (top view): (1) electrodynamic shaker, (2) shaker stinger, (3) force transducer, (4) customized adapter, (5, 6) reference accelerometer, (7) tapping tool, (8) CTTVS and (9) MLC *Softsynchro 3*

Table 3 Measuring equipment for frequency response analysis

Pos	Description	Type
1	Electrodynamic Shaker	*LDS V101*
3	Force transducer	*PCB 208C03*
5/6	uniax. Accelerometer	*B &K 4507*
-	DAQ	*NI-9234*
-	Signal Generator	*Creative SB X-Fi*
-	Shaker Amplifier	*FA TPA3116*
-	Analysis Software	*MATLAB 2021b*

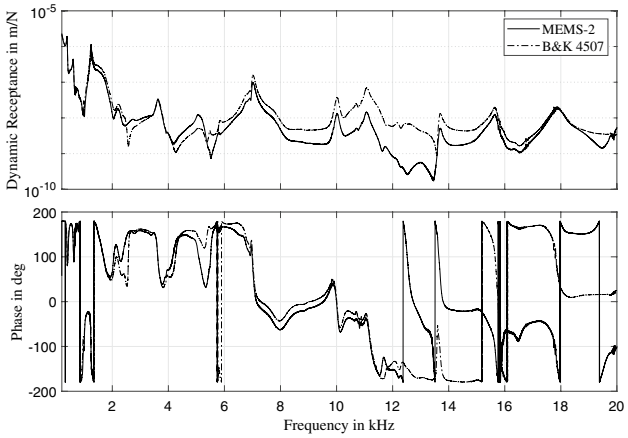

Fig. 12 Comparison of FRF between MEMS-2 and reference accelerometer mounted at CTTVS housing

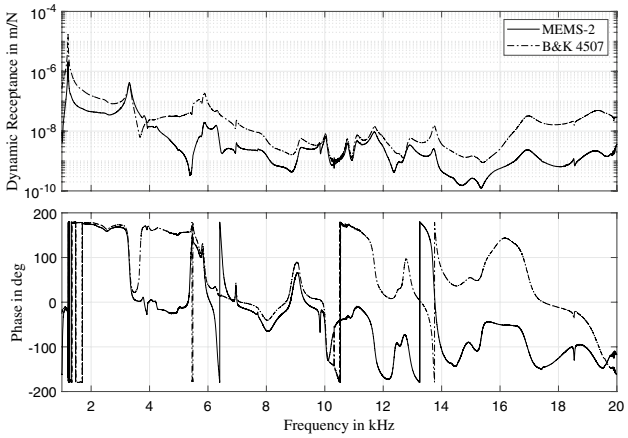

Fig. 13 Comparison of FRF between MEMS-2 and reference accelerometer mounted at tapping tool

type of rigid connection allows a proper excitation of the tapping tool in radial *y*-axis direction, whereby the forced vibrations are induced at the chamfer and guiding section of the tapping tool.

A linear sinusoidal sweep excitation was chosen to ensure reasonable quality of the FRF measurement, even in the presence of unknown non-linearities [20]. Further, the reference accelerometer is applied by using a thin layer of *Brüel & Kjaer* bees wax, which provides a flat response function in the frequency bandwidth of interest [21]. The measurement equipment used for the frequency response analysis is listed in Table 3.

The output signal of the CTTVS, the reference accelerometer as well as the force transducer is acquired by a sound and vibration purposes DAQ-Device of type *NI-9234*, since a data acquisition using the telemetry unit without additional amplifiers is not possible due to missing measuring channels and interface requirement such as IEPE standard. However, the telemetry unit provides same data acquisition characteristics as the *NI-9234* regarding sample rate and resolution, which is a reasonable trade-off. Since we are interested in the verification of the CTTVS by means of FRF analyis, the transfer function of the signal processing stage $G_1(\mathrm{i}\omega)$ for level adjustment and anti-aliasing filter, which implemented on the telemetry unit, can be ignored. Thus, the FRF analysis is considering

$$H(\mathrm{i}\omega) = \left(\prod_{k=1}^{8} H_k(\mathrm{i}\omega)\right) H_\mathrm{p}(\mathrm{i}\omega)$$

whereby $H_\mathrm{p}(j\omega)$ represents parasitic impacts.

Figures 12 and 13 shows for both spatial configurations of the reference accelerometer the FRF (dynamic receptance) considering only the MEMS accelerometer in

y-axis direction, denoted as MEMS-2. The results are averaged over 10 measurements.

Further, the sine sweep excitation frequency was set to 1 kHz-20 kHz with a duration of 20 s, whereby the max. Force amplitude was 10 N due to limitations of the electrodynamic shaker. To provide a proper overall estimation, the H_v -Estimator is chosen and calculated via the *modalfrf(.)*-function provided by the *MATLAB Signal Processing Toolbox*.

Comparing the dynamic receptance of the MEMS-2 and reference accelerometer, a reasonable accordance can be observed with regard to the frequency positions of peaks for both spatial configurations of the reference accelerometer. Furthe, the curve progression also shows good accordance, which is also applicable to the phase diagram. Since, in the first configuration the reference accelerometer was attached to the housing of CTTVS, eigenfrequencies of the housing structure can influence the dynamic receptance by the presence of additional peaks or different magnitudes, compared to the measurements when the reference accelerometer was attached to the tapping tool directly.

However, the results of the experimental frequency response analysis proves the suitability of the CTTVS for detecting eigenfrequencies of the tapping tool up to 20 kHz. This is justified by max. excitation force amplitude of 10 N, which is lower than cutting edge forces measured in thread cutting experiments with a tap size of M8x1.25 mm and workpiece material of type 42CrMo4, which are also considered in this contribution [22].

5 Thread cutting experiments

Thread cutting experiments are carried out on a vertical machining center of type *DMC850v* using a M8x1.25 mm high-speed steel tapping tool and workpiece material of type 42CrMo4. According to the recommendations of the tool manufacturer, a cutting speed of 15 $\frac{\text{m}}{\text{min}}$ is chosen which yields a spindle speed of 597 rpm and a feed rate of 12.4 $\frac{\text{mm}}{\text{s}}$. The manufacturing of the core holes is carried out using unused solid carbide drills with internal cooling to provide appropriate core hole quality. Due to missing sealing of the electronic components of the sensor-integrated tap holder, the application of internal and external cooling during thread cutting is not possible. Hence, the core holes are filled with cooling lubricant before thread cutting experiments were carried out as shown in Fig. 14.

During thread cutting experiments, the raw bit stream of the close-to-tool vibration sensor is acquired with the max. sample rate of 51.2 kHz and stored on the telemetry unit's SDCard for post analysis. In the following, only the output of the MEMS-2 accelerometer of the CTTVS is considered. The time waveform for a single thread is shown in Fig. 15.

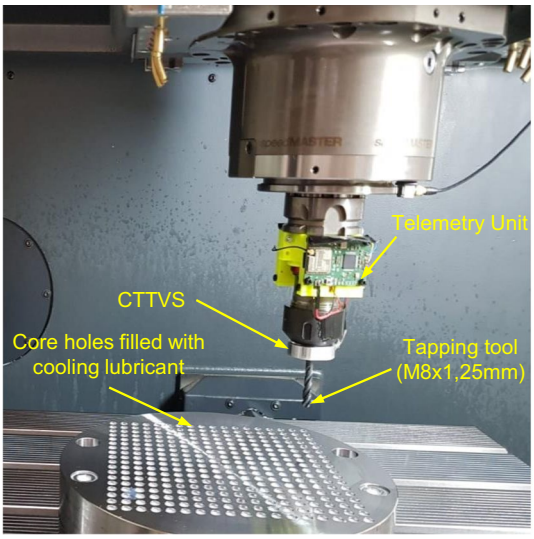

Fig. 14 Setup of the thread cutting experiments

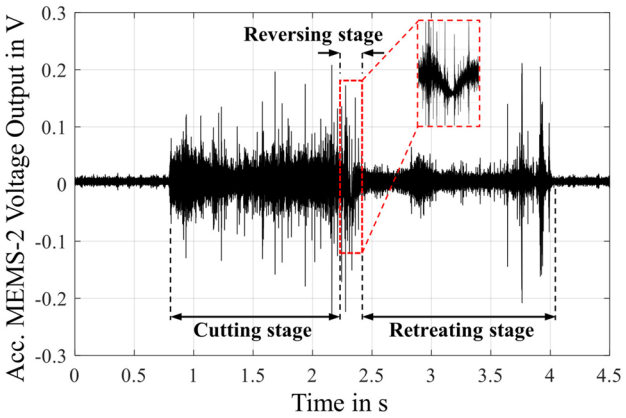

Fig. 15 Time waveform of a single thread cutting process

The close-to-tool vibration signal can be divided into three stages which are the cutting stage, the reversing stage and the retreating stage. It is obvious, that during the entire cutting stage, the amplitude is higher compared to the retreating stage.

This is plausible since the cutting forces during the chip removal within the cutting stage induces higher amount of vibrational excitation energy in the tapping tool than during the retreating stage where frictional forces at the thread flanks are dominating. Further, the reversing of spindle rotational direction is observable. However, the time waveform proves the unsteady character of the tapping process which forces analysis methods in the time-frequency domain such as the Short Time Fourier Transform (STFT). Squaring the STFT magnitude yields the spectrogram of the power spectral density (PSD) which is considered in this contribution. To improve the signal-to-noise ratio (SNR), the spectrogram

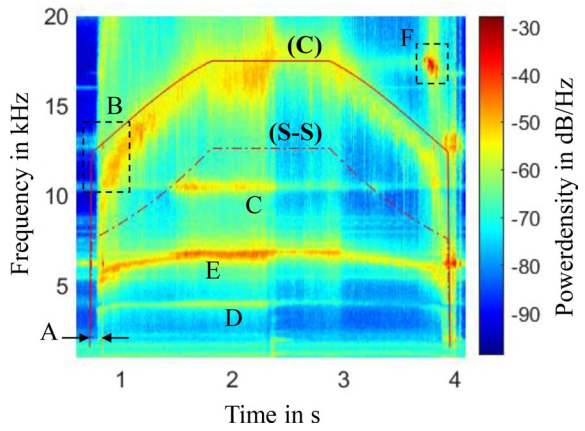

Fig. 16 Averaged PSD spectrogram of MEMS-2 accelerometer

of the PSD is averaged over 18 tapping processes yielding a clearer slope of the instantaneous frequency. The PSD spectrogram of the MEMS-2 accelerometer is shown in Fig. 16, whereby the underlying magnitude is the voltage output of the MEMS accelerometer. Further, the results of the estimated instantenous eigenfrequency of the tapping tool considering the workpiece-tool contact as clamped (C) and simply supported (S-S) are inserted in the spectrogram.

It can be seen clearly that the clamped condition **(C)** is fitting closer to the instantenous eigenfrequency measured by the CTTVS than considering a simply supported boundary condition between the workpiece and the tapping tool. However, there is a deviation of **(C)** in curve shape shown in region B, and in time represented by A. One reason for this deviation may the simplification of tapping tool geometry considered for the analytical approach, since the exact tool geometry contains a tapered geometry in the chamfer section, as shown in Fig. 1. Next, the analytical approach does not consider frequency decreasing damping effects such as the friction between the guidance section of the cutting edges and the workpiece. Additionally, the analytical approach does not include the mass of CTTVS, which will also decrease the tapping tool fundamental flexural eigenfrequency, even considering the CTTVS being attached close to the clamped boundary of the collet chuck. Further, the underlying system boundary for the analytical approach depicted in Fig. 2 is not considering the dynamics of other components such as the tool holder. The spectrogram shows a second instantaneous frequency E with narrower bandwidth at lower frequencies, which is not further investigated in this contribution but assumed as the torsional instantaneous eigenfrequency of the tapping tool. Besides this, horizontal lines with higher power density such as C and D can be assumed as excited eigenmodes of the entire system with steady modal parameters, which are independent of the thread cutting process.

6 Conclusion and outlook

In this contribution an analytical approach for estimating the instantaneous eigenfrequency of the tapping tool's fundamental flexural vibration is derived. The geometry of the tapping tool is simplified by means of a segmented beam system with different circular diameters considering the *Euler-Bernoulli* beam theory. Further, the sensor-integrated tap holder including the Close-To-Tool Vibration Sensor (CTTVS) based on MEMS accelerometers is introduced. The focus is put on the CTTVS with regard to the functional principle and the verification by means of experimental frequency response analysis using an electrodynamic shaker with broadband excitation. The measured frequency response functions yielded a reasonable compliance between the MEMS-accelerometer based CTTVS and a piezoelectric reference accelerometer. Based on this results, thread cutting experiments are carried out, whereby the close-to-tool vibration signals is analysed in the time-frequency-domain. The results obtained from the PSD spectrogram are:

- The tapping tool-workpiece contact considered as a clamped **(C)** boundary condition shows a better compliance between the analytically and experimental results of the instantaneous eigenfrequency than considering a simply supported **(S-S)** contact.
- Deviation in curve shape of the instantaneous eigenfrequency between analytically and experimental results are present which can be justified by the underlying simplification of the tapping tool used for the analytically approach with regard to geometry and boundary conditions.
- Excitation of eigenmodes are observed based on the presence of horizontal lines with higher power density independent of the process time.

However, further investigations should be considered in future studies:

- Using different types of workpiece material to investigate the experimental impact of the material properties on the instantaneous eigenfrequencies in context of the tapping tool-workpiece contact.
- Considering an elastic support or foundation (e.g. Winkler [23]) for modelling the tapping-tool-workpiece contact as an improvement point of the analytically approach.
- Examination of the PSD spectrogram regarding additional instantaneous eigenfrequencies, such as the assumed torsional vibration mode marked with E, and the occurrence of *hot spots* such as region F shown in Fig. 16.

- Impact of process uncertainties such as synchronisation error, axis offset or faulty core diameter on the instantaneous eigenfrequency of the tapping tool's fundamental flexural vibration. The latter can be utilised for process monitoring purposes of the tapping process.

Appendix A Coefficient matrix of the analytically approach considering tapping tool-workpiece contact as clamped boundary condition

$$\boldsymbol{A} = \begin{pmatrix} \left[t_{1j}^{(n)}(0)\right]^{\epsilon\mathbb{R}^{2\times4}}_{\substack{j=1,\dots,4\\ n=0,1}} & [0]^{\epsilon\mathbb{R}^{2\times4}} & [0]^{\epsilon\mathbb{R}^{2\times4}} \\ \left[t_{1j}^{(n)}(\beta_1 l_1)\right]^{\epsilon\mathbb{R}^{2\times4}}_{\substack{j=1,\dots,4\\ n=0,1}} & -\left[t_{2j}^{(n)}(0)\right]^{\epsilon\mathbb{R}^{2\times4}}_{\substack{j=1,\dots,4\\ n=0,1}} & [0]^{\epsilon\mathbb{R}^{2\times4}} \\ I_1\left[t_{1j}^{(n+2)}(\beta_1 l_1)\right]^{\epsilon\mathbb{R}^{2\times4}}_{\substack{j=1,\dots,4\\ n=0,1}} & -I_2\left[t_{2j}^{(n+2)}(0)\right]^{\epsilon\mathbb{R}^{2\times4}}_{\substack{j=1,\dots,4\\ n=0,1}} & [0]^{\epsilon\mathbb{R}^{2\times4}} \\ [0]^{\epsilon\mathbb{R}^{2\times4}} & \left[t_{2j}^{(n)}(\beta_2 l_2)\right]^{\epsilon\mathbb{R}^{2\times4}}_{\substack{j=1,\dots,4\\ n=0,1}} & -\left[t_{3j}^{(n)}(0)\right]^{\epsilon\mathbb{R}^{2\times4}}_{\substack{j=1,\dots,4\\ n=0,1}} \\ [0]^{\epsilon\mathbb{R}^{2\times4}} & I_2\left[t_{2j}^{(n+2)}(\beta_2 l_2)\right]^{\epsilon\mathbb{R}^{2\times4}}_{\substack{j=1,\dots,4\\ n=0,1}} & -I_3\left[t_{3j}^{(n+2)}(0)\right]^{\epsilon\mathbb{R}^{2\times4}}_{\substack{j=1,\dots,4\\ n=0,1}} \\ [0]^{\epsilon\mathbb{R}^{2\times4}} & [0]^{\epsilon\mathbb{R}^{2\times4}} & (\boldsymbol{C}):\left[t_{3j}^{(n)}(\beta_3 l_3)\right]^{\epsilon\mathbb{R}^{2\times4}}_{\substack{j=1,\dots,4\\ n=0,1}} \end{pmatrix} \tag{A1}$$

Acknowledgements This document contains results of the research project SFB 805 (Projektnummer 57157498) funded by Deutsche Forschungsgemeinschaft (DFG, German Research Foundation).

Funding Open Access funding enabled and organized by Projekt DEAL.

References

1. Ahn JH, Lee DJ, Kim SH, Kim HY, Cho KK Effects of synchronizing errors on cutting performance in the ultra-high-speed tapping 52(1):53–56. https://doi.org/10.1016/S0007-8506(07)60529-0. Accessed 2020-08-04
2. Polvorosa R, de Lacalle LNL, Egea AJS, Fernandez A, Esparta M, Zamakona I Cutting edge control by monitoring the tapping torque of new and resharpened tapping tools in inconel 718 106(9): 3799–3808. https://doi.org/10.1007/s00170-019-04914-5. Accessed 2020-08-04
3. Öztürk T, Sarıaya E, Weigold M Sensor-integrated tap holder for process uncertainty detection based on tool vibration and axial length compensation sensors. https://doi.org/10.1007/s00170-021-07825-6. Accessed 2021-10-04
4. Mastering Uncertainty in Mechanical Engineering. https://doi.org/10.1007/978-3-030-78354-9. https://link.springer.com/10.1007/978-3-030-78354-9 Accessed 2022-04-14
5. Ma Y-C, Wan M, Yang Y, Zhang W-H Dynamics of tapping process 140:34–47. https://doi.org/10.1016/j.ijmachtools.2019.02.002. Accessed 2020-08-04

6. Matsuda R, Shindou M, Hirogaki T, Aoyama E Research and Development Group, Yamamoto Metal Technos Co., Ltd. 4-7 Setoguchi, 2-chome, Hirano-ku, Osaka 547-0034, Japan, Department of Mechanical Engineering, Doshisha University, Kyotanabe, Japan: Monitoring of rotational vibration in tap and endmill processes with a wireless multifunctional tool holder system 12(6):876–882. https://doi.org/10.20965/ijat.2018.p0876. Accessed 2021-10-04
7. Bleicher F, Ramsauer CM, Oswald R, Leder N, Schoerghofer P Method for determining edge chipping in milling based on tool holder vibration measurements 69(1):101–104. https://doi.org/10.1016/j.cirp.2020.04.100Accessed 2022-05-03
8. Ramsauer C, Bleicher F New method for determining single cutting edge breakage of a multi-tooth milling tool based on acceleration measurements by an instrumented tool holder, 67–77. https://doi.org/10.36897/jme/131918. Accessed 2022-05-03
9. Moehring H-C, Nguyen QP, Kuhlmann A, Lerez C, Nguyen LT, Misch S (2016) Intelligent tools for predictive process control. Procedia CIRP 57:539–544. https://doi.org/10.1016/j.procir.2016.11.093
10. Li X, Liu X, Yue C, Liang SY, Wang L Systematic review on tool breakage monitoring techniques in machining operations 176:103882. https://doi.org/10.1016/j.ijmachtools.2022.103882. Accessed 2022-05-03
11. SCHUNK GmbH & Co. KG: iTendo^2. https://schunk.com/de_de/startseite/itendo2/#c296959
12. Dogra A, Kapoor S, DeVor R (2002) Mechanistic model for tapping process with emphasis on process faults and hole geometry. Journal of Manufacturing Science and Engineering-transactions of The Asme - J MANUF SCI ENG 124. https://doi.org/10.1115/1.1430237
13. Oezkaya E, Biermann D Development of a geometrical torque prediction method (GTPM) to automatically determine the relative torque for different tapping tools and diameters 97(1): 1465–1479. https://doi.org/10.1007/s00170-018-2037-3. Accessed 2022-04-15
14. Ahmadi K, Ahmadian H Modelling machine tool dynamics using a distributed parameter tool-holder joint interface 47(12):1916–1928. https://doi.org/10.1016/j.ijmachtools.2007.03.004. Accessed 2022-04-17
15. Mallik AK, Kher V, Puri M, Hatwal H On the modelling of non-linear elastomeric vibration isolators 219(2):239–253. https://doi.org/10.1006/jsvi.1998.1883
16. Graff KF (1991) Wave Motion in Elastic Solids. Dover Books on Physics Series. ISBN: 0198561180
17. Gorman DJ (1975) Free Vibration Analysis of Beams and Shafts, ISBN: 0471317705 Place: New York. A Wiley-Interscience publication, Series
18. Jang SK, Bert CW Free vibration of stepped beams: Exact and numerical solutions 130(2):342–346. https://doi.org/10.1016/0022-460X(89)90561-0
19. Szabo I (1956) Höhere Technische Mechanik. Springer-Verlag, Berlin, Göttingen, Heidelberg
20. Gloth G, Sinapius M (2003) Detection of non-linearities in swept-sine measurements. In: XXI International Modal Analysis Conference (IMAC), Orlando/Florida, USA, 3-6 February 2003. https://elib.dlr.de/14523/
21. Broch JT (1984) Mechanical Vibration and Shock Measurements, Soborg - Denmark. ISBN: 8787355345. https://www.bksv.com/doc/bn1330.pdf
22. Geßner F, Weigold M, Abele E (2020) Measuring and modelling of process forces during tapping using single tooth analogy process. Production Engineering 15. https://doi.org/10.1007/s11740-020-01004-4
23. Karnovsky IA (2004) Non-classical Vibrations of Arches and Beams: Eigenvalues and Eigenfunctions. McGraw-Hill Engineering reference guide series, New York. 0071431888